공학석사학위논문

공간적으로 분해된 레이저-유도 플라즈마의 발광 스펙트럼 분석

Emission Spectrum Analysis of Spatially-Resolved Laser-Induced Plasma

2017년 2월

서울대학교 대학원

기계항공공학부

배 상 은

공간적으로 분해된 레이저-유도 플라즈마의 발광 스펙트럼 분석

Emission Spectrum Analysis of Spatially-Resolved Laser-Induced Plasma

지도교수 도 형 록

이 논문을 공학석사 학위논문으로 제출함

2016 년 10 월

서울대학교 대학원

기계항공공학부

배 상 은

배상은의 공학석사 학위논문을 인준함

2016 년 12 월

위 원 장 고 승 환 (인)

부위원장 도 형 록 (인)

위 원 송 한 호 (인)

Abstract

Emission Spectrum Analysis of Spatially-Resolved Laser-Induced Plasma

Sangeun Bae
School of Mechanical and Aerospace Engineering
The Graduate School
Seoul National University

A laser-induced plasma (LIP) is one-dimensionally resolved along a laser line and temporal evolution of the emission spectra at each position of LIP are obtained. A plasma is generated by focusing pulsed-laser (2^{nd} harmonics of ND:YAG) just above a jet nozzle supplying dry air during the experiments to avoid any interferences between laser pulses. A 85 *mm* Nikon camera lens mounted on a translational stage collects the emitted photons from LIP and focuses it onto an entrance slit of a spectrometer with a magnification factor of 10 to improve spatial resolution. The region of interest (ROI)—a section of the LIP of which its emission is illuminated into the spectrometer—is varied by translating the lens. A thickness of the

ROI is estimated to 10 μm considering a slit width and the magnification factor. A spatial interval and a total length are 0.1 *mm* and 3.0 *mm*, respectively. A gate time of an intensified CCD is fixed at 10 *ns* and a gate delay is varied from 100 to 400 *ns* with a constant interval of 10 *ns* after laser arrival to observe temporal evolution of the emission spectrum. As a result, the intensity matrix is given by a function of wavelength (a spectral range is from 650 to 780 *nm*), position, and gate delay. The spectral range is chosen because it includes neutral oxygen (O I) lines used for plasma temperature calculation and neutral/singly ionized nitrogen lines (N I/N II) which are useful in evaluating a relative abundance of neutral atoms and ions. A plasma temperature distribution and its temporal evolution are estimated by the local thermodynamic equilibrium (LTE) assumption and the Boltzmann analysis. Two neutral oxygen lines at 715.67 and 777.19 *nm* are used for the Boltzmann analysis. The result shows a non-uniformity in plasma temperature and a gradual decay of overall temperature during the experiments (gate delay from 100 to 400 *ns*). On the other hand, a total intensity distribution is also calculated by summing up the spectral intensities. Strong total intensity regions are not matched with that of high temperature. In contrast, high temperature regions are more likely to have a stronger ionized nitrogen line at 661 *nm* compared to a neutral nitrogen line at 746 *nm*.

Keywords: Laser-induced breakdown spectroscopy (LIBS), laser-induced plasma, plasma temperature, spatially-resolved plasma

Student Number: 2015-20729

Contents

List of Tables

List of Figures

1. Introduction

1.1. Laser-induced breakdown spectroscopy

Laser-induced breakdown spectroscopy (LIBS) is one of the most widely used measurement methods using laser because of its minimal system complexity and great signal-to-noise ratio (SNR). Furthermore, it is also a great advantage that any seeder particles which might be unable to completely follow turbulent flows are not required in LIBS while they are necessary in other laser diagnostics techniques, e.g., particle image velocimetry (PIV) or laser Doppler anemometry (LDV). Therefore, LIBS is a greatly helpful measurement method especially in a turbulent flow.

In LIBS, a plasma is generated by focusing pulsed-laser in a gaseous medium. An extremely strong irradiance (approx. 100 GW/cm^2, [1]) induces the multiphoton ionization of neutral molecules in a gas. Once free electrons are produced by the multiphoton ionization, they absorb photons much more easily than neutral species: this photon energy absorption of free electrons is called the inverse-Bremsstrahlung (IB) process. Then, the excited electrons resulted from the IB process not only ionize other neutral species but also dissociate large molecules (breakdown), and the numbers of ions and electrons are exponentially increasing.

Some physical properties of the species in a laser focal volume can be inferred by analyzing the emission spectrum of LIP because optical properties of the emitted photons from LIP are determined by the physical/chemical characteristics of their origins. For example,

wavelengths of emitted photons depend on the internal structure of species due to quantized energy levels. Pressure is also a major determinant of spectrum and simultaneously one of the most crucial properties in engineering problems. Thus, a lot of approaches have been utilized to analyze LIP emission spectra.

In previous research, it is shown that peak intensities and line broadenings are closely related to atomic compositions and pressure of a plasma plume respectively [2, 3]. The relationship between atomic abundance and their emission intensities are intuitively understandable. The more atoms would give the stronger emission. On the other hand, line broadening is primarily due to the Stark-broadening caused by the interactions among electrons and ions in plasma [3]. The broadened line shape, thus, is affected by electron number density, and the ambient pressure could be inferred from the properties of line shapes, e.g., line width.

Since the development of a pulsed-laser with sufficient power for generating plasma in a gas, LIBS has become a practical non-intrusive measurement method having a little possibility of flow perturbation. Especially, its excellent SNR enables the experiments with a short measurement time. Sufficiently short measurement time could minimize uncertainty due to fast flows. A short-gated (a few tens of *ns*) LIBS was conducted for quantitative fuel concentration measurements in supersonic flows [4]. The order of nanoseconds is also short enough to examine a reactive gas mixture before reaction actually occurs because the high enthalpy chemistry has a timescale in the order of microseconds. To ensure low uncertainty and high accuracy, LIBS experiments in a reactive

gas like an air-fuel mixture should be conducted within a microsecond of the total measurement time. Otherwise LIP would initiate combustion, and this leads to considerable changes of ambient gas conditions, e.g., increase in temperature and pressure.

1.2. Limitation of LIBS

Focused laser beam induces not only ionization but also dissociation. This is inevitable in LIP because an extremely strong irradiance is required to form LIP due to small photon absorption cross sections of neutral molecules. After the multiphoton ionization is initiated, generated free electrons gain a lot of energy from incoming photons by the IB process. They possess significantly high energy levels, thus collisions between the electrons and neutral molecules or ions would lead to dissociation of large species. Though atomic peak intensities from LIP emission spectrum considerably depend on atomic composition of plasma, the information on parent species could hardly be examined. Kazunobu Kobayashi et al. investigated LIP emission from hydrocarbon fuel mixtures [5]. They conducted LIBS in several different gas mixtures consisted of the same atomic compositions using oxygen, carbon dioxide, helium, nitrogen and hydrocarbons (CH_4, C_2H_4, C_3H_8, and C_4H_8). The results showed the almost identical spectra and their temporal evolution despite of differences in parent species. Figure 1.1 shows an example of the identical spectra from two different gaseous mixture composed of the same atomic composition (the compositions are given in Table 1.1). If molecules in a mixture have

different atomic composition individually—for example, a mixture of dry air and methane (composed of O_2, N_2, and CH_4)—, estimating methane concentration or equivalence ratio is possible by regarding nitrogen and hydrogen atom line as representatives air and fuel respectively, because each one is a dominant atom of air and fuel [6]. In some potential environments, however, this method could hardly be applicable. For example, in a gas mixture undergoing chemical reactions, to determine molecular compositions at a laser focal point by analyzing LIP emission spectra is difficult because reactants, products, and even reactant/product mixtures all have the identical atomic compositions which lead to the similar emission spectra.

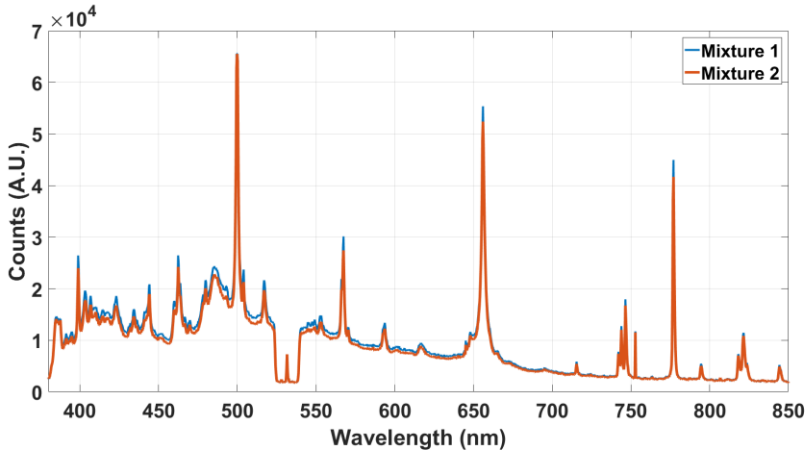

Figure 1.1. Emission spectra from LIP generated in two different gaseous mixtures composed of the same atomic compositions. Their compositions are given in Table 1.1.

Table 1.1. Atomic and molecular compositions of two different gaseous mixtures. Mixture 1 contains ethylene while methane and carbon dioxide are contained in Mixture 2.

% by volume	Mixture 1	Mixture 2
N_2	77.4%	77.4%
O_2	20.6%	18.6%
CH_4	–	2.0%
C_2H_4	2.0%	–
CO_2	–	2.0%
C	1.9%	1.9%
H	3.8%	3.8%
O	19.8%	19.8%
N	74.4%	74.4%

1.3. Motivation

A majority of physical phenomena in engineering fields account for molecular levels. For example, combustion instability and flame propagation velocity depend on molecular structures of fuels. Though LIBS is one of the most useful measurement techniques, however, it is an obvious limitation that only atomic lines could be observed from the conventional LIBS. This limitation would be a huge disadvantage to many experimental areas.

In this study, LIP is one-dimensionally resolved and the emission spectra are acquired at each position of plasma to identify spatial variation. This is a starting point for discovering an influence of molecular structures to LIP emission spectrum. Because it is evident that LIP is gradually quenched due to interaction with surrounding molecules, e.g., nitrogen or oxygen molecules in the atmosphere, and the emission spectrum from the plasma boundary would be affected by those molecules.

2. Experimental setup

2.1. Overall

Figure 2.1 shows a schematic of the overall experimental setup. A second harmonic Nd:YAG laser at 10 *Hz* (Continuum Powerlite 8000) was focused by a plano-convex lens (f = 30.0 *mm*) and generated plasma just above a nozzle exit. An adjustable half-wave plate and a polarizing plate beamsplitter (extinction ratio of 10,000:1 and transmission efficiecny of P-pol > 95%) were used to control laser power while maintaining beam profile. A splitted beam was directed to a power detector (Gentec-EO UP19-VR), and its power was monitored during expriments (by Gentec-EO Tuner). Focused laser energy was constant at 50 *mJ/pulse* throughout the experiments. Dry air was continously supplied through a nozzle with a jet velocity of approx. 30 *m/s* to blow-off the any plasma remainder (a plasma could be affected by the former one because laser is supplied at 10 *Hz*). The jet velocity was rougly calculated with a cross-sectional area of the nozzle and a volume flow rate measured by a flowmeter. Photons emitted from LIP were collected by a 85 *mm* Nikon lens and focued onto a spectrometer inlet (Acton Research SP300i) passing through a notch filter (center wavelength = 532 *nm*, bandwidth = 17 *nm*) to protect a CCD from scattered laser photons. Photons dispersed inside the spectrometer were captured by an intensified CCD (Princeton Instruments PI-MAX). All signal timings were syncronized by a delay generator (Stanford Research Systems DG535) and verified using an oscilloscope (Keysight MSO3000).

A gate width of ICCD was fixed at 10 *ns* while a gate delay (time after laser arrival at a focal point) was varied from 100 to 400 *ns* with an interval of 10 *ns* to observe temporal evolution of spectra. The minimum gate dealy of 100 *ns* was chosen to avoid strong continuum emission from LIP.

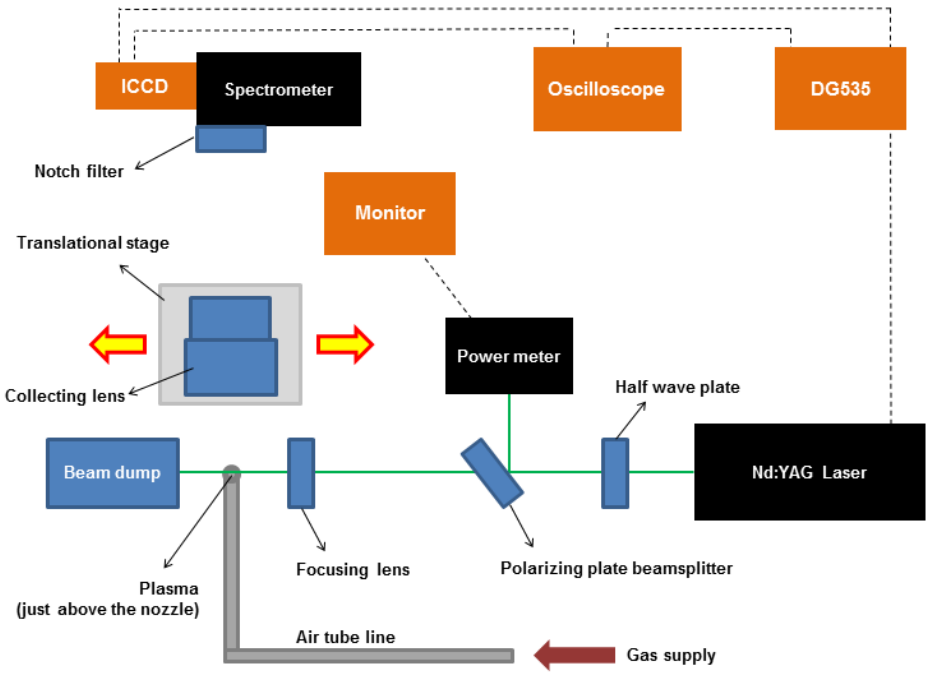

Figure 2.1. A schematic of the experimental setup for spatially-resolved LIP emission spectra observation.

2.2. Lens alignment for spatially-resolved plasma

A collecting lens was mounted on a translational stage which was able to translate along the laser line (Figure 2.2). In contrast to the conventional LIBS experiments, LIP was focused onto an entrance slit as a magnified image (a magnification factor was 10) in this study. As the lens translates, the image on the slit also follows it. Therefore, a section of LIP locating on the slit was able to be adjusted. A region of interest upon LIP under the observation at that time could be verified precisely by reading a gradation of a micrometer on the translational stage. Because the slit width and the magnification factor were 100 μm and 10 respectively, a plasma slice with a thickness of 10 μm was under an observation at a time. The total length of LIP was estimated to about 2.0 *mm*. The micrometer of the translational stage was adjusted from 0 to 3.0 *mm* (whole plasma was able to be observed within this range) with a resolution of 0.1 *mm*. An overall experimental setup and specifications are tabulated in Table 2.1.

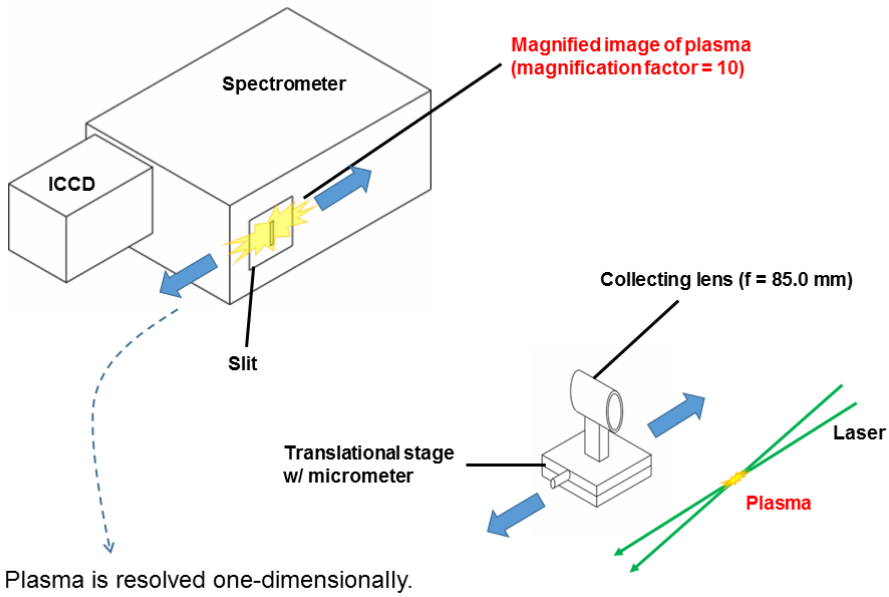

Figure 2.2. LIP is focused onto an entrance slit of a spectrometer as a magnified image at a magnification factor of 10. The image is able to translate along a laser line because it follows a collecting lens mounted on a translational stage.

Table 2.1. An overall experimental setup and specification of the experiments.

Laser source	2^{nd} harmonics ND:YAG laser at 532 *nm* 250 *mJ/pulse* (50 *mJ* to focus & 200 *mJ* to powermeter)
Spectrometer	300 *g/mm* blazing at 500 *nm* Calibrated by a Ne lamp Slit width = 100 μm
ICCD	10 *ns* gate width Varied gate delays Averaged over 30 laser shots
Gas	Dry air (30 *m/s*)
Spatial resolution	100 μm
Temporal resolution	10 *ns*

3. Results and discussion

Spectral intensities at every gate delay and each position of LIP were obtained as a result of the experiments. As previously mentioned, the minimum gate delay of 100 *ns* was chosen to avoid continuum emission (Figure 3.1). Figure 3.2a shows temporal evolution of LIP emission spectrum at a fixed position (x = 1.6 *mm*), while spatial variation of the spectrum at a gate delay (t_d = 100 *ns*) is shown in Figure 3.2b. Any spectrum does not appear outside the plasma.

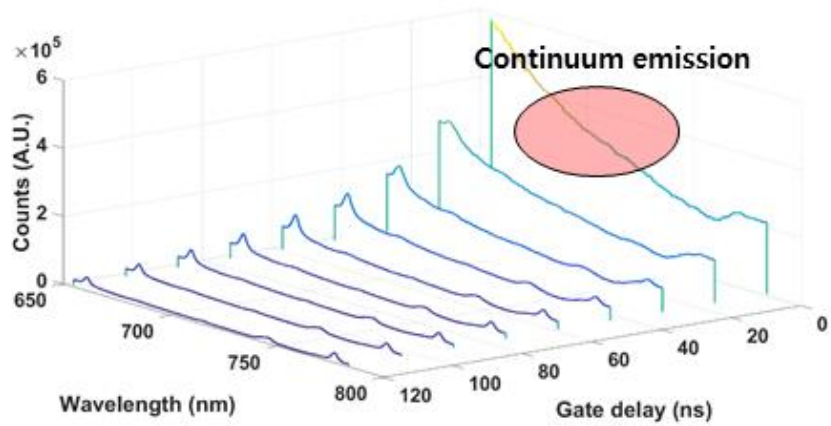

Figure 3.1 Temporal evolution of LIP emission spectrum in early phase ($t_d \leq 120\ ns$). Continuum emission is observed in early plasma.

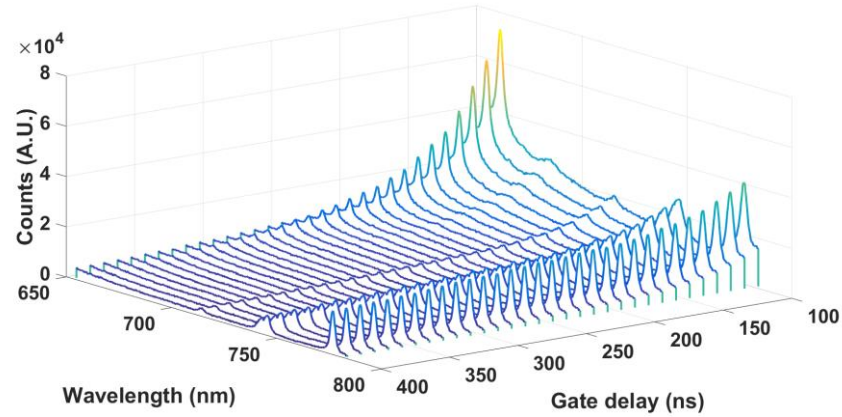

(a)

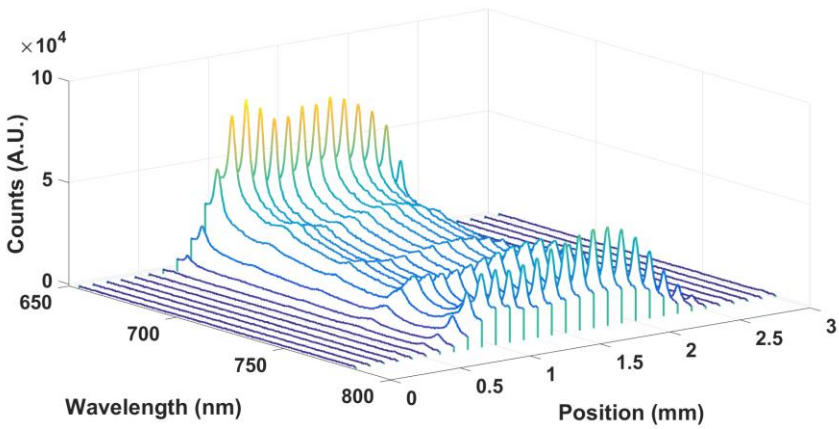

(b)

Figure 3.2 (a) Temporal evolution of LIP emission spectrum at $x = 1.6\ mm$, and (b) spatial variation of the spectrum at $t_d = 100\ ns$.

3.1. Plasma temperature distribution

Plasma temperature is calculated by the Boltzmann analysis [5]. An emission intensity by the radiative transition from k–th state to i–th state, I_{ki}, is given by,

$$I_{ki} = n_k A_{ki} h\nu_{ki} \tag{1}$$

n, A, h, and ν indicates population, the Einstein coefficient, the Planck constant, and frequency respectively. Then, population of excited species to the energy level, E_k, is illustrated in Eq. (2) and a ratio of two intensities is given in Eq. (3).

$$n_k = \frac{n_0 g_k \exp(-\frac{E_k}{kT})}{Z(T)} \tag{2}$$

$$\frac{I'}{I} = \frac{n_0' g' A' \nu' \exp(-\frac{E'}{kT'})}{n_0 g A \nu \exp(-\frac{E}{kT})} \cdot \frac{Z(T)}{Z'(T')} \tag{3}$$

Where, n_0, g, k, Z, and T denote number density of species, degeneracy, the Boltzmann constant, a partition function, and temperature. If an intensity ratio in Eq. (3) is accounted for two atomic line emission from the same species, then $n_0 = n_0'$ and $Z = Z'$. On the other hand, Hazem El–Rabii et al. verified that local thermodynamic equilibrium (LTE) assumption is valid for early ($t_d \leq 3\ \mu s$) air plasma [7]. Therefore, temperatures of all the species within plasma are the same, then T becomes plasma temperature and $T = T'$. Rearranging Eq. (3) with LTE assumption yields,

$$T = \frac{E' - E}{k \ln \frac{I g' A' \nu'}{I' g A \nu}} \tag{4}$$

Two intensities could be acquired from captured spectra and the other values available in NIST database [8]. From the spectral range observed from this study, two neutral oxygen atomic lines at 715.67 and 777.19 *nm* are used for plasma temperature calculation, because former one is undisturbed by any other line. Although 777.19 *nm* line is superimposed with closely spaced the other two lines (see Figure 3.3), contributions of each lines could be estimated with their degeneracies, the Einstein coefficients, and frequencies by assuming that their upper level energy levels, E_k, are the same. Then, contribution of 777.19 *nm* line for 777 *nm* triplet is given by,

$$C_{777.19} = \frac{I_{777.19}}{\sum_j I_j} = \frac{g_{k,777.19} A_{ki,777.19} \nu_{ki,777.19}}{\sum_j g_{k,j} A_{ki,j} \nu_{ki,j}} = 46.68\% \tag{5}$$

Before taking $I_{777.19}$ and $I_{715.67}$ from the spectra, baseline correction should be conducted to eliminate background signals due to dark currents in an ICCD and free-to-free transition of highly excited species regardless of atomic structures. Figure 3.4 shows an example of a fitted baseline.

The local maximum values near 715 and 777 *nm* lines from baseline corrected spectra substitute I and I' in Eq. (3). The other values from NIST database are tabulated in Table 3.1. Figure 3.5 shows the resultant plasma temperature distribution along the laser line and their temporal evolution. The estimated temperature varies from 25,000 to 50,000 K depending on the position and the time. The region having signal intensities

of 715.67 or 777.19 *nm* lines less than 36.8 % of their maximum values is not contoured, because plasma temperature at this region is inappropriate to be calculated by the Boltzmann analysis which requires atomic emission. It is shown that the overall temperature gradually decays as time passes. However, the temperature distribution at each timing is asymmetric about its maximum temperature position (approx. 1.1 *mm*).

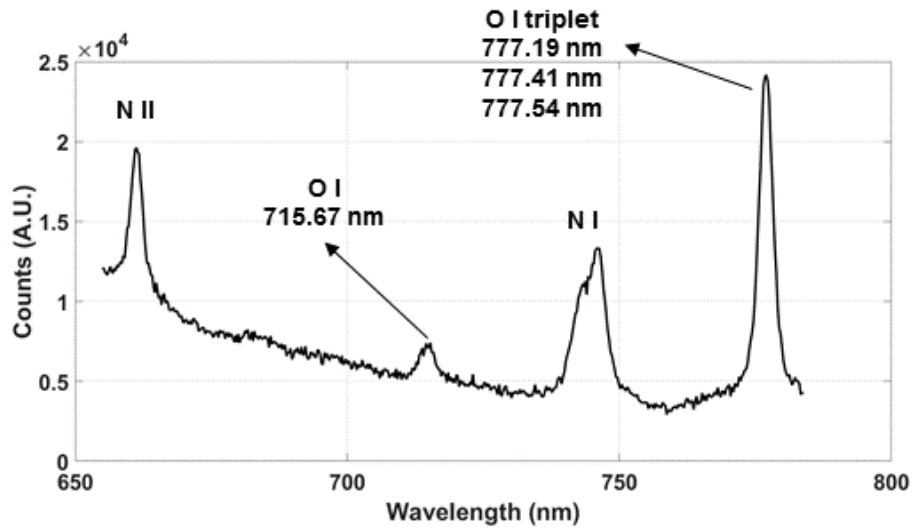

Figure 3.3. Emission spectrum of spatially−resolved LIP at x = 1.5 *mm*, t_d = 200 *ns*, and t_g = 10 *ns*. O I triplet at 777 *nm* is a superimposed line of three individual closely spaced lines of O I.

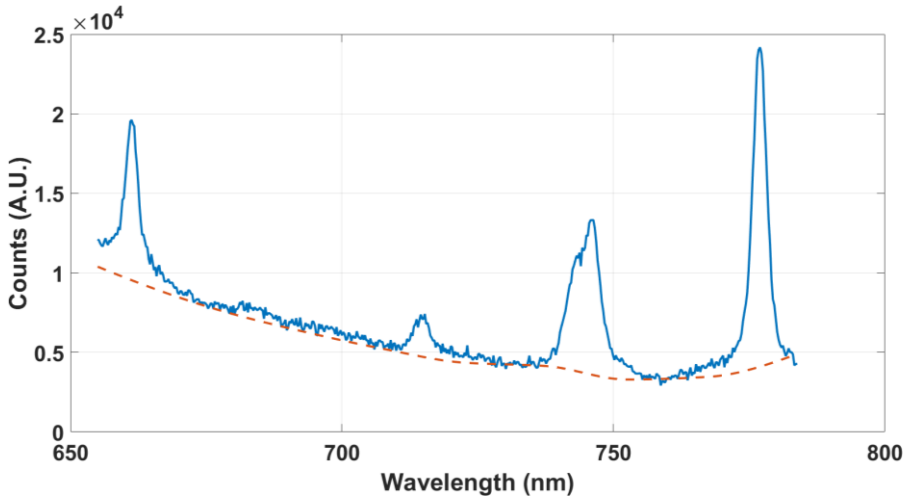

Figure 3.4. Raw spectrum from (blue solid line) and fitted baseline (red dashed-line). All of the conditions are same with that in Figure 3.1.

Table 3.1. The Einstein coefficients (A_{ki}), upper level energies (E_k), and degeneracies (g_k) of four neutral oxygen atomic transitions [8].

λ (nm)	A_{ki} (s^{-1})	E_k (eV)	g_k
715.67	5.05e+07	14.4604126	5
777.19	3.69e+07	10.7409313	7
777.41	3.69e+07	10.7404755	5
777.54	3.69e+07	10.7402250	3

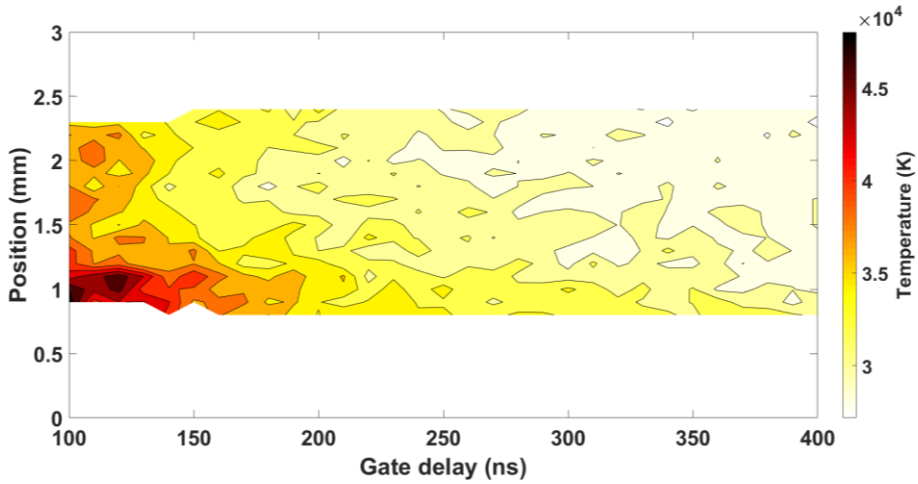

Figure 3.5. Plasma temperature distribution and its temporal evolution. Temperature is calculated by the Boltzmann analysis under LTE assumption using 715.67 and 777.19 *nm* neutral oxygen lines. Poor signal regions (signal intensities are less than 36.8% of the maximum) are not contoured.

3.2. Total/spectral emission intensity distribution

Total emission intensity distribution and its temporal evolution are given by summing up spectral intensities at each position and timing (Figure 3.6). It is clearly observed that high temperature region in Figure 3.5 and strong total intensity region in Figure 3.6 are not matched. Although the detector used in this study is a nonlinear CCD (spectral sensitivity depends on wavelength), total emission intensity could be regarded as a number of species which are sufficiently excited to emit photons because the spectral range of interest (from 650 to 780 *nm*) is narrow. Thus, it is verified that high temperature does not indicate large population of excited species. For example, plasma temperature/total emission intensity at 1.0 and 2.0 *mm* when a gate delay is 100 *ns* are 48,040 *K* / 1.14e+07 and 36,310 *K* / 1.11e+07 respectively. Plasma temperature at 2.0 *mm* is 75.6% of the temperature at 1.0 *mm*, while total emission intensity at 2.0 *mm* is almost comparable to that at 1.0 *mm* (97.4%).

Figure 3.7a and 3.7b shows nitrogen line emission intensities at 746 and 661 *nm* respectively. The former one is neutral nitrogen (N I) line while the other one is singly ionized nitrogen (N II) line. Nevertheless, line emission intensity is not linearly proportional to a number of species undergoing a radiative transition emitting photons possessing the wavelength of the line, it could be considered as a qualitative measure for the number of the species because they are strongly dependent on each other. Therefore, strong emission intensity region in Figure 3.7a has a large population of neutral nitrogen atoms. It is noticed that the preferable

regions of N I and N II are completely distinguishable. The strong N II region is matched with the high temperature region (compare Figure 3.5 and 3.7b). In spite of the greater maximum intensity in N II (4.5E+4) compared to that of N I (1.6E+4), N II emission intensity is rapidly weakened and becomes zero after 250 *ns* when the plasma temperature quenches to less than 35,000 *K*. This relationship between plasma temperature and a population of N II indicates that ionization of a neutral atom requires additional energy and results in higher temperature.

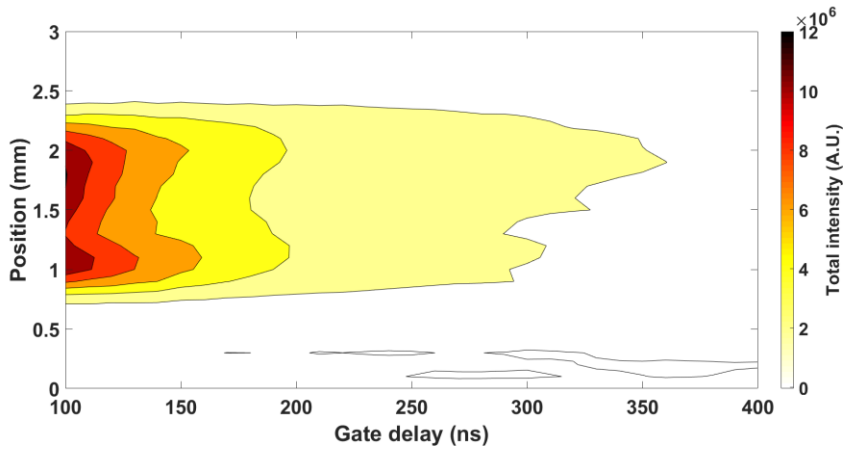

Figure 3.6. Total emission intensity distribution and its temporal evolution.

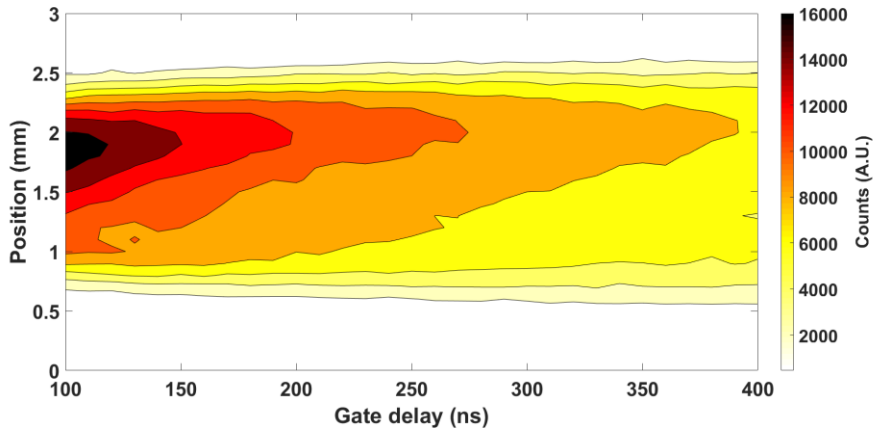

(a)

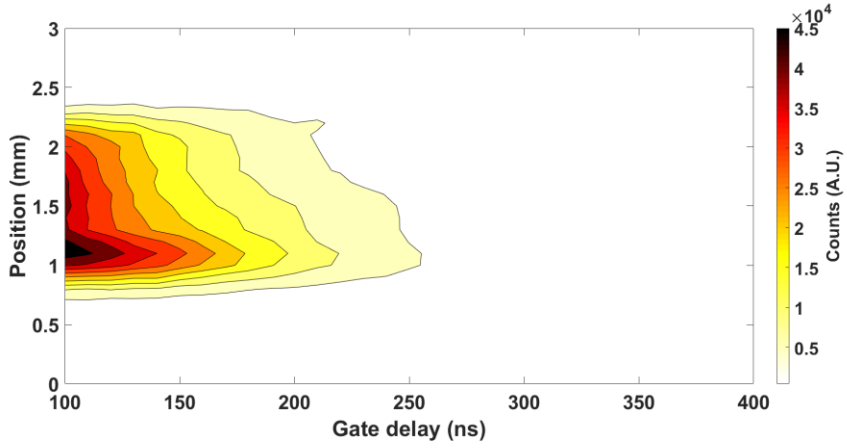

(b)

Figure 3.7. Spectral emission intensity distribution and its temporal evolution: (a) neutral atomic nitrogen line (N I) at 746 *nm* and (b) singly ionized nitrogen line (N II) at 661 *nm*.

3.3. Emission spectra from a low temperature plasma

There are two ways to observe emission spectra from a low temperature plasma: i) waiting for a LIP to be quenched, and ii) selectively observing cold region of a LIP. The first one is a temporal approach, while the second one is a spatial way. Figure 3.8 shows temporal evolution of the averaged plasma temperature at the entire, cold, and hot regions of the LIP. The cold and hot regions are chosen to be 1.9~2.1 and 0.9~1.1 *mm* respectively. The measured data points are represented by a marker 'X' and each set of data points from individual region is fitted and represented by dashed-lines. By capturing the emission from the cold region of a LIP, the emission spectra from a cold temperature plasma can be obtained in early timing. For example, a gate delay of approximately 230 *ns* is required to acquire the emission spectra from the entire plasma at 32,000 *K* (see a black dashed-line in Fig. 3.8). On the other hand, the plasma temperature in the cold region reaches to 32,000 *K* in a gate delay of approximately 180 *ns*.

The relative intensities and their temporal evolution of N I line at 746 *nm* for each region are plotted in Figure 3.9. The emission intensities of N I are normalized by the maximum values—at the earliest timing (a gate time of 100 *ns*)—of the respective region. Therefore, this figure shows the decay rate of N I line at the individual region, although their absolute intensities are inappropriate to be compared because of a difference in physical sizes of the region of interests: the hot and cold regions have a length of 0.2 *mm*, while the entire plasma is about 2.0 *mm* long. As a result,

it is verified that the cold region and the entire plasma have almost identical decay rates in N I line during the observed timing (a gate delay from 100 to 400 *ns*). The hot region shows a slower decay than the other two. I conjecture that this difference is due to ionized nitrogen in the hot region. As plasma temperature decreases by quenching, some of N II in the hot region recombine with electrons and become N I. These neutral nitrogen atoms are still excited enough to emit photons. The hot region, consequently, shows a lower decay rate in N I line than the cold region which has a fewer number of N II due to relatively low temperature.

From Figure 3.8 and 3.9, it is verified that the cold region and the entire plasma have distinct temperature and similar decreasing aspects in relative intensities of N I. So the cold region gives less decayed N I emission than the entire plasma when we investigate an emission spectrum at a certain plasma temperature. For example, it is estimated from the fitted curves in Figure 3.8 that gate delays of 185 and 227 *ns* are required for reaching plasma temperature of 32,000 *K* at the cold region and the entire plasma respectively. The cold region at 185 *ns* has 77.3% of the maximum intensity, but the entire plasma at 227 *ns* has 69.8% which is quite less than that of the cold region. Figure 3.10 shows differences between gate delays of the entire plasma and the cold region depending on temperature. This gap in gate delay exponentially increases as temperature decreases, which means a gate delay for the entire plasma should be even much longer compared to the cold region to observe a lower temperature plasma emission spectrum. This longer gate delay results in weakened emission intensities (see Figure 3.9). Thus, stronger signal intensities from low

temperature plasmas could be achieved by selectively observing cold regions of plasmas and taking shorter gate delays compared to the conventional LIBS (which does not conduct spatially-resolved emission spectra analysis).

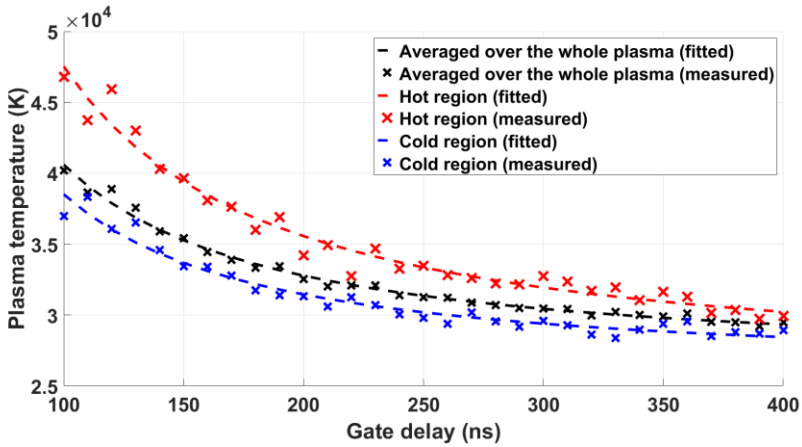

Figure 3.8. Temporal evolution of plasma temperature depending on regions of a LIP. Black, red, and blue indicate values averaged over the whole LIP, the hot, and the cold regions respectively. Markers 'X' are the measured values, and the each fitted curve is plotted by dashed-lines.

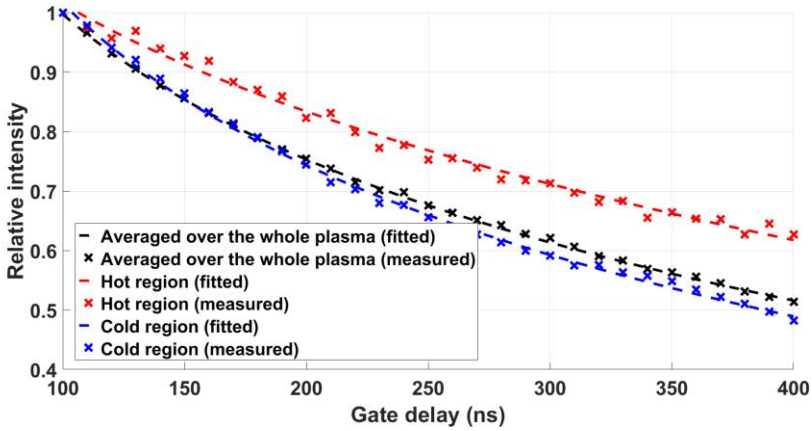

Figure 3.9. Temporal evolution of relative intensities of N I line at 746 *nm* depending on regions of a LIP. N I emission intensities are normalized by the maximum intensity from each region. The respective colors and markers denote the same meanings with that in Figure 3.8.

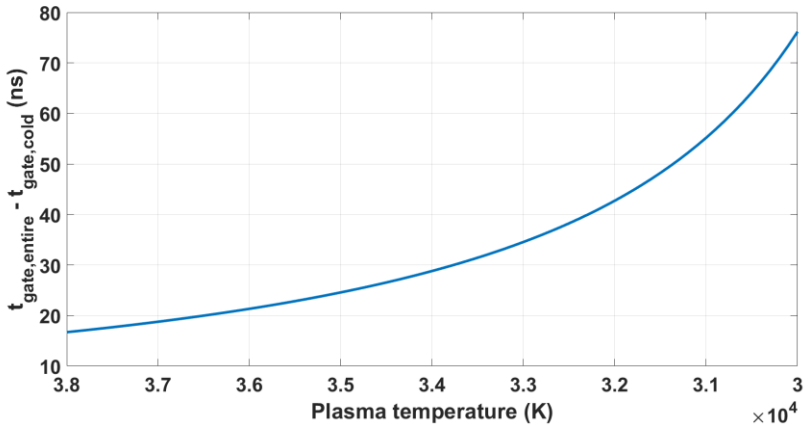

Figure 3.10. A difference between required gate delays of the entire plasma and the cold region depending on plasma temperature.

4. Conclusion

A LIP was imaged onto an entrance slit of a spectrometer as a magnified image (magnification factor was 10) using a convex lens. The lens mounted on a translational stage enabled spatially-resolving the LIP. A spatially-resolved LIP emission spectra analysis conducted in this study gave spatial variation in plasma temperature and its temporal evolution. The LTE assumption and the Boltzmann analysis were used to estimate plasma temperature. By comparing temperature distribution and spectral—N I at 746 *nm* and N II at 661 *nm*—intensity distribution, it was verified that the hot region had more nitrogen ions than the cold region. In contrast, the cold region had more neutral nitrogen atoms than the hot region. I conjecture that additional energy required to ionize neutral atoms (in other word, ionization energy) accounts for this contrasting difference. Therefore, it is also presumed that emission spectra affected by molecular structures should be observed from plasmas at low temperature which might have species without dissociation. It is already reported that very weak molecular band emission could be observed at a gate delay over approx. 3 μs when a plasma becomes sufficiently quenched. This study suggested a strategy to investigate emission spectra from quenched plasmas with shorter gate delays when emission intensity still remains stronger than the conventional method (to observe the whole plasma), and the strategy was to selectively observe the cold region of a LIP rather than to have a long gate delay. Decay rates of a neutral nitrogen atom line at 746 *nm* observed from the cold region and the entire plasma were

compared as an example. The result showed that the cold region could have much shorter gate delays than the entire plasma when observing emission spectra from plasmas at the same temperature. Because this study dealt with the lowest temperature of approx. 28,000 K, molecular band emission analysis which could be conducted with plasmas at much lower temperature remains as a future work.

References

[1] David A. Cremers, Leon J. Radziemski, "Handbook of Laser-Induced Breakdown Spectroscopy 2nd Ed.," Wiley

[2] Moon Soo Bak, Brendan McGann, Campbell Carter, Hyungrok Do, "Determinants of Laser-Induced Breakdown Spectra in N2-O2 Mixtures," J. Phys. D: Appl. Phys. 49 (2016) 125202 (10pp)

[3] S. Yalcin, D.R. Crosley, G.P. Smith, G.W. Faris, "Influence of Ambient Conditions on the Laser Air Spark," Appl. Phys. B 68, 121-130 (1999)

[4] Hyungrok Do, Campbell D. Carter, Qili Liu, Timothy M. Ombrello, Stephen Hammack, Tonghun Lee, Kuang-Yu Hsu, "Simultaneous Gas Density and Fuel Concentration Measurements in a Supersonic Combustor Using Laser Induced Breakdown," Proceedings of the Combustion Institute 35 (2015) 2155-2162

[5] Kazunobu Kobayashi, Moon Soo Bak, Hiroki Tanaka, Campbell Carter, Hyungrok Do, "Laser-Induced Breakdown Emission in Hydrocarbon Fuel Mixtures," J. Phys. D: Appl. Phys. 49 (2016) 155201 (7pp)

[6] Hyungrok Do, Campbell Carter, "Hydrocarbon Fuel Concentration Measurement in Reacting Flows Using Short-Gated Emission Spectra of Laser Induced Plasma," Combustion and Flame 160 (2013) 601-609

[7] Hazem El-Rabii, Sergey B Victorov, Azer P Yalin, "Properties of an Air Plasma Generated by Ultraviolet Nanosecond Laser Pulses," J. Phys. D: Appl. Phys. 42 (2009) 075203 (10pp)

[8] Kramida, A., Ralchenko, Yu., Reader, J., and NIST ASD Team (2015). NIST Atomic Spectra Database (ver. 5.3), [Online]. Available:

http://physics.nist.gov/asd [2016, December 6], National Institute of Standards and Technology, Gaithersburg, MD.

초록

공간적으로 분해된 레이저-유도 플라즈마의 발광 스펙트럼 분석

서울대학교 대학원
기계항공공학부
배상은

레이저-유도 플라즈마(LIP)를 레이저 라인 방향을 따라 일차원적으로 공간 분해하여 관찰하였고, 각 위치에서의 방출 스펙트럼과 각 스펙트럼의 시간에 다른 변화를 얻었다. 플라즈마는 볼록 렌즈를 이용하여 ND:YAG 펄스 레이저를 노즐 출구에 집중시킴으로써 생성하였으며, 플라즈마에 대한 레이저 펄스 간의 간섭을 피하기 위해 노즐을 통해 건조 공기를 지속적으로 공급하였다. 레이저 라인을 따라 축 이동이 가능한 스테이지 위에 설치된 85 *mm* Nikon 렌즈를 이용해 LIP 방출광을 집적하였으며, 공간적 분해능을 향상시키기 위해 확대계수 10을 갖는 확대상을 분광기의 슬릿에 형성하였다. LIP의 어느 부분을 관찰하느냐는 스테이지를 조절하여 렌즈를 이동시키고, 따라서 분광기 슬릿에 입사되는 이미지의 위치를 조절하여 결정하였다. 슬릿 폭과 확대계수를 고려하면 전체 플라즈마 길이 중에서 한 번에 10 μm 두께 부분만을 관찰하는 것이라고 계산된다. LIP 이미지를 0.1 *mm*씩 움직이며 매 위치마다 스펙트럼을 얻었고, 전체 측정 범위는 3.0 *mm*이다. Intensified CCD의 gate time은 10 *ns*으로 일정하였으

며, 방출 스펙트럼의 시간에 따른 변화를 관찰하기 위해 gate delay는 100부터 400 *ns* 사이에서 10 *ns*씩 변화시키며 실험하였다. 그 결과로 파장, 위치, 그리고 gate delay의 함수로 표현되는 강도 행렬을 얻었다. 관찰한 파장 범위는 650에서 780 *nm* 사이인데, 그 이유는 해당 범위 안에 플라즈마 온도 계산에 이용되는 중성 산소 원자(O I) 방출선과 중성 원자와 이온의 상대적인 수를 비교할 수 있는 중성 질소 원자(N I)와 1가 질소 이온(N II)의 방출선이 포함되기 때문이다. 실험을 통해 얻은 강도 행렬을 기반으로, LTE 가정과 Boltzmann 해석을 통해 플라즈마 온도의 공간적 분포와 시간에 따른 변화를 계산하였다. Boltzmann 해석에는 715.67과 777.19 *nm*에 위치한 두 개의 중성 산소 원자 방출선들이 이용되었다. 결과적으로, 균일하지 않은 플라즈마 온도 분포와 관찰한 시간 범위 (gate delay 100에서 400 *ns* 사이) 내에서 전체적인 온도의 지속적인 감소가 확인되었다. 한 편, 파장별 세기(spectral intensity)를 모두 합산하여 전 세기(total intensity)의 분포 또한 계산하였다. 플라즈마 상에서 전 세기가 강한 부분이 높은 온도를 갖는 지역과 일치하지는 않았다. 반면에 높은 온도의 지역은 746 *nm*에 위치한 중성 질소 원자 발광선보다 661 *nm*에 위치한 1가 질소 이온 발광선이 더 강한 경향을 보였다.

요약어: 레이저-유도 분해 분광학 (LIBS), 레이저-유도 플라즈마, 플라즈마 온도, 공간적으로 분해된 플라즈마

학번: 2015-20729